Simulation of Sloshing-Shear Mixed Shallow Water Waves (II) Numerical Solutions

Weihao Chung*, Iau-Teh Wang and Yu-Hsi Hu

Abstract—This is the second part of the paper. It, aside from the core subroutine test reported previously, focuses on the simulation of turbulence governed by the full STF Navier-Stokes equations on a large scale. Law of the wall is found plausible in this study as a model of the boundary layer dynamics. Model validations proceed to include velocity profiles of a stationary turbulent Couette flow, pure sloshing flow simulations, and the identification of water-surface inclination due to fluid accelerations. Errors resulting from the irrotational and hydrostatic assumptions are explored when studying a wind-driven water circulation with no shakings. Illustrative examples show that this numerical strategy works for the simulation of sloshing-shear mixed flow in a 3-D rigid rectangular base tank.

Keywords—potential flow theory, sloshing flow, space-time filtering, order of accuracy.

I. INTRODUCTION

AS shown in the first part of the paper, the hydrostatic assumption has been modified into a dynamic one and all eddy viscosity terms have been retained in order to relax the restrictions of potential flow theory. Equations have been also discretized explicitly in the horizontal direction, and the terms of the horizontal derivatives have been grouped together to form a forcing function regarding the scale of shallow fluid flows in the horizontal direction, which was relatively larger than in the vertical direction. Following the numerical models developed in the first part, this study has dealt with the strategy of numerical calculations, such as setting boundary conditions close to a solid wall and deciding solution procedures for the target variables. The possibility that the Smagorinsky-Lilly "constant" employed by different researchers varied with flow cases and could be much smaller than that determined by Lilly [1] has been estimated as well. More than five flow cases were investigated in this study, not only for model validation but also for robustness. It is then possible to realize how the

Dr. Weihao Chung is an associate professor of the Department of Civil Engineering, Chinese Military Academy, Kaohsiung, Taiwan, R.O.C., 1, Wei-wu Road, Fengshan City, Kaohsiung County, 83059, Taiwan, R.O.C., (Corresponding author. Tel.:+886-7-745-6290; e-mail: weihao5@yahoo.com.tw).

Iau-Teh Wang teaches at the Department of Civil Engineering, Chinese Military Academy and is a Ph.D. postgraduate student of Graduate Institute of Disaster Prevention on Hillslopes and Water Resources Engineering, National Pingtung University of Science and Technology, Pingtung, Taiwan, R.O.C., 1, Wei-wu Road, Fengshan City, Kaohsiung County, 83059, Taiwan, R.O.C. (e-mail address: wang55992002@yahoo.com.tw).

Yu-hsi Hu is a lecturer of the Department of Applied English, Tajen University, Taiwan, R.O.C. (e-mail address: e-mail: gracehu17@gmail.com).

hydrostatic assumption and the restriction of potential flow theory affect the turbulent flow behavior in our simulations. Model applicability was finally tested by simulating a sloshing-shear mixed water flow where the viscous forces and the dynamic pressure acted simultaneously and were of the same importance. In the present study, all water flows were restricted in a rigid prismatic tank without a roof.

II. STRATEGY OF NUMERICAL CALCULATIONS

A. Prescription of Boundary Conditions

At solid walls, the non-slip boundary condition is not necessarily obeyed. Furthermore, the imposition of a non-slip boundary condition would require the resolution of the viscous sub-layers, which would translate into an unbearable computational burden. Since detailed boundary layer dynamics are not of interest for most large eddy simulations, solid wall boundary conditions are specified by employing an approach similar to the one applied by Deardorff [2] and Mason and Callen [3] , which is based on the use of the law of the wall. Strictly speaking, the law of the wall is only valid for ensemble averaged values of steady velocity fields. Nevertheless, as argued by Mason and Callen [3], inertia terms are negligible in the neighborhood of the wall. Departures from ensemble averaged to space-time filtered velocities will be small. Consequently, the law of the wall was plausible in this study as a model of the boundary layer dynamics. A little effort leads to a Robin-type expression of the following form at the bottom of the lake:

$$\left.\frac{\partial u}{\partial z}\right|_{z=\Delta} = \frac{\sqrt{C_f}}{\sqrt{2}\kappa\Delta}u\big|_{z=\Delta} \tag{1}$$

with the roughness coefficient being:

$$C_f = \frac{2\kappa^2}{\ln^2(\Delta/z_0)} \tag{2}$$

where z_0 = roughness height, κ = von-Karman's constant = 0.41, and Δ = the outer edge of boundary layer, i.e., a distance from the wall which is sufficiently larger than the viscous sub-layer thickness and sufficiently small for the law of the wall to hold as a good approximation [4]. After taking a finite difference discretization, Eq. (1) can be reformed as an explicit

World Academy of Science, Engineering and Technology
International Journal of Civil and Environmental Engineering
Vol:5, No:2, 2011

function of $u|_{z=\Delta}$ being obtained without iteration. Expressions similar to Eq. (1) can be rewritten for vertical walls.

B. Selection of C_{SL}

The Smagorinsky-Lilly turbulence model contains two important parameters, the eddy constant C_{SL} and the filtering length λ_s. Since eddy viscosity estimated by the model is proportional to the squared product of C_{SL} and λ_s, calibration of the two parameters has its importance. Lilly [1] pointed out that, analogous to the von Karman's constant in the viscous sub-layer, C_{SL} is a constant (≈ 0.17) in the inertia sub-range where fluid flow is essentially homogeneous and isotropic, and the balance between eddy production and viscous dissipation is expected. Thus, grid size cannot be too large or small such that the corresponding wave number falls outside the inertia sub-range. It is also well known that for shear flows the value has to be smaller [2] and that for wall-bounded flows the value has to be a function of the distance from the wall [3]. In practice, the C_{SL} value is adjusted, however, by trial-and-error until reasonable numerical solutions result. For example, Bedford and Babajimopoulos [5] selected a C_{SL} value of 0.005 so that the computed eddy viscosity smoothly transmitted and reached a steady state without causing numerical divergence. Schmidt and Schurmann [6] set C_{SL} =0.165 to perform a large-scale simulation of the atmospheric boundary layer. The difference between the two values was large in spite of minor variations being given to λ_s. Liao et al. [7] suggested that C_{SL} ranged between 0.1 and 0.5, and adopted 0.17 to simulate the vertical jets in a cross flow field. Chung [8] showed that C_{SL} was constant in the inertia sub-range, but possibly varied for wind-induced shear flows with $\Psi_i = 0$. Therefore, it seemed reasonable to adopt a C_{SL} value different from 0.17 in engineering practices, but to view 0.17 as typical (refer to the Appendix of Part I).

C. Numerical Analysis Procedures

After setting the C_{SL} value and boundary conditions, the resulting (fully discrete) algebraic system was manipulated to yield a linear system of pentadiagonal matrix equations, each corresponding to a specific position on a horizontal plane. In other words, each matrix equation was composed of the vertically aligned grid nodes associated with the same (x,y) coordinate. Equations were thus decoupled in the horizontal direction, along which nodal values could be borrowed from those of the previous time steps. An efficient, direct back substitution solver was implemented for the solution of these systems.

The fully discretized version of Eqns. (10), (11), (13) and (16) resulted in a system of nonlinear algebraic equations which, in the Picard iteration environment, could be solved according to the following procedures: i) solving the horizontal momentum, Eq.(10), for $u^{n+1,k}$ and $v^{n+1,k}$ with k representing the iteration number, and the pressure information lagging by one iteration; ii) solving the modified continuity, Eq.(13), for $w^{n+1,k}$, which proceeds as step i) on uncoupled vertical lines; iii) determining the total water depth $H^{n+1,k}$ from Eq. (16); and iv) finally solving the vertical momentum, Eq.(11), for $P^{n+1,k}$ by integration. For step i), since the horizontal dynamics were treated explicitly in Eq. (10), coupling only existed for nodal values that were vertically aligned. Procedures i) - iv) were repeated until the preset convergence criteria for all target variables were satisfied. Computations were then advanced to the next time step. It is noteworthy that a rigorous criterion $|w^{n+1} - w^n|/|w^n| < 0.00001$ was set for w, regarding w as the most sensible variable to iterations. Before satisfying the criterion, five to seven iterations were generally required for each time step. The solution strategy thus avoided the constitution of the Poisson equation for the calculation of pressure, which involves a significant mathematical burden.

III. MODEL VERIFICATIONS

Wave computations have been organized into figures in this section. Each figure consists of several subfigures, to which letters (a), (b), (c) and so on are assigned in left-to-right, up-to-down order.

A. Validation of Shear Flow

As a diagnostic test for the above developed numerical models involving wind shears, simulations of a stationary turbulent Couette flow governed by

$$0 = \frac{\partial}{\partial z}\left(\nu \frac{\partial u}{\partial z} - \overline{u'w'}\right) = \frac{\partial}{\partial z}\left(G \frac{\partial u}{\partial z}\right) \qquad (3)$$

were performed in a wide channel with a depth of h and a flat bottom. Eq. (3) was obtained from Eq. (2) by dropping all the acceleration terms, pressure gradients, and Ψ_i, if the flow in x and y was uniform. Eq. (3) implies the total shear stress $\tau/\rho (= G\partial u/\partial z)$ is constant in z and so is the shear velocity $u_* = \sqrt{\tau/\rho}$ for an incompressible flow. Assume now that the flow consists of three parts in the channel: sub-layer, wall layer, and velocity defect layer, in which the velocity distributions are usually described, respectively, by $\partial u/\partial z \sim u_*^2/\nu$, $\partial u/\partial z \sim u_*/(\kappa z)$, and $\partial u/\partial z \sim (\tau/\rho)/G$. Let the sub-layer range from 0 to $\Delta (\to 0)$, and the wall layer occupy a thickness of z_d. Eventually, $G = u_* hz/(s*z_d)$ and $G = u_* h/s$, with s being a proportional constant, is plausible in the wall layer and the velocity defect layer, respectively. Using $s=17$, the velocity distribution is expressed by:

$$u = \frac{u_*}{\kappa}\ln\left(\frac{z}{z_0}\right) \qquad (4)$$

in the wall layer, and

World Academy of Science, Engineering and Technology
International Journal of Civil and Environmental Engineering
Vol:5, No:2, 2011

$$u = \frac{u_*}{\kappa}\ln\left(\frac{z}{z_0}\right) + 17u_*\left(\frac{z-z_d}{h}\right) \quad (5)$$

in the velocity defect layer. Eqs. (4) and (5) are obtained also by directly integrating Eq. (3) using the specified G. Thus, for $z_d = 0.145h$, the velocity at the free water surface ($z=h$) is given by:

$$u_s = \frac{u_*}{\kappa}\left[\ln\left(\frac{0.145h}{z_0}\right) + 6.94\right] \quad (6)$$

Let the channel have a length of 1000 m (x-direction), width of 1000 m (y-direction), and mean depth of 2 m (z-direction). The following discretization characteristics were used: $\Delta x = \Delta y = 100$ m, $\Delta z = 0.2$ m, $\Delta t = 10$ sec., and $z_0 = 0.01$ m. Boundary conditions at x=0 m and x=1000 m were zero x-gradients, while the boundary conditions at the bottom of the lake and at y=0 and y=1000 m were the simulated law of the wall applied at a distance of $\Delta = 0.02$ m. On the free water surface, there was assumed to be a constant wind shear stress. By experience, wind shear stress is often expressed as $\tau_w = C_{10}\rho_a|V_r|V_r$ [9] with ρ_a the air density, C_{10} the drag coefficient referring to the conventional anemometer height of 10 m, and V_r the relative velocity of the wind speed to the fluid at the water surface. Recent data [10] has suggested that the C_{10} given by $C_{10} = 1.6\times10^{-3}$ for $V_r \leq 7m/s$ and $C_{10} = 2.5\times10^{-3}$ for $V_r \geq 10m/s$. Thus, a typical wind stress of $0.1N/m^2$ resulting from a wind speed of $7m/s$ was obtained.

Since K_t was decomposed into several terms when discretizing Eq. (3), the model validation proceeded with the presets of $C_{SL} = 0$ and $\nu = G$ in our program code. By doing so, what we solved turned out to be Eq .(3), and Eq. (5) was then used to compare with the numerical solution. Figure 4 shows the time evolution of the u profile associated with the channel center. The flow profile was being produced by a constant wind shear stress of 0.5 N/m^2 ($=\tau$) applied to initially quiescent water. The solid line represents the analytical solution (6). As expected, the computed results (symbols) at various time levels gradually matched the steady state solution (solid line). Changing the Δ and τ values yielded different velocity profiles that all approached the corresponding analytical solution as time passed, attesting again to the model's accuracy.
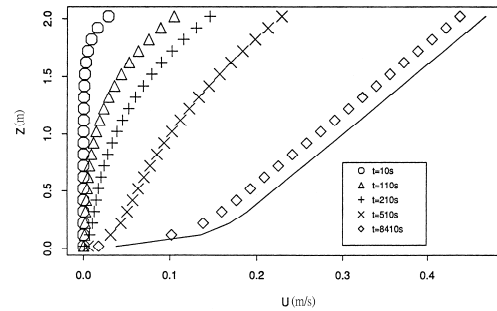

Fig. 4 Time evolution of the x-component velocity profiles (symbols). Solid line represents the analytical solution associated with the steady state Couette flow.

B. Validation of Sloshing Flow

In this subsection, the flow dimensions chosen were L=100 m, B=50m and D=10 m, with L, B, and D as the length, width, and water depth, respectively. The grid node numbers equaled 11 in both x and y directions and 31 in the z-direction. Other related parameters were $\rho = 1000$ kg/m3, $z_0 = 0.01$ cm, $\Delta = 0.03$ cm, $\Delta t = 0.2$ second, and $C_{sL}/C_{sL0} = 0.01$, where C_{sL0} corresponded to a theoretically determined value (refer to Chung [11]).

When a rectangular rigid water tank shifts only along the x direction, and the shift can be defined as $x(t) = c\sin(\omega t)$, a one-dimensional change in the water level can occur over time. Many scholars, such as Faltinsen [12], Okamoto and Kawahara [13] and Chen et al. [14], have discussed this phenomenon. Wu et al. [15] cited the linear solution of velocity potential found from the results of Faltinsen [12] to validate their own models. The linear solution of water elevation reads (there is a typo for E_n in Wu et al. [15]):

$$\eta = \frac{c}{g}\left(x\omega^2 + \sum_{n=0}^{\infty}C_n\omega\sin k_n x\right)\sin\omega t - \frac{c}{g}\sum_{n=0}^{\infty}\omega_n\left(C_n + \frac{E_n}{\omega^2}\right)\sin k_n x\sin\omega_n t \quad (7)$$

where

$$k_n = \frac{(2n+1)\pi}{L}, \quad \omega_n^2 = gk_n\tanh k_n D, \quad E_n = \omega^3\frac{4}{L}\frac{(-1)^n}{k_n^2},$$

and $C_n = \frac{E_n}{\omega_n^2 - \omega^2}$.

As admitted by Faltinsen et al. [16], the linear theory itself describes only qualitatively well the measured elevation of swirling waves frequently appearing close to tank walls and turning potentially in a rotational motion. Though their solutions in general were limited by several factors, Eq. (7) has been employed here for solution validation, as cited by Wu et al. [15].

Figure 5 with a c value of 0.00183 shows the comparison between the linear solution and the simulated water level of the

World Academy of Science, Engineering and Technology
International Journal of Civil and Environmental Engineering
Vol:5, No:2, 2011

water tank during the shift at $\omega/\omega_0 = 0.9$, 1.1, and 0.99. It was found that in Figure 5 all the numerical solutions compared favorably with Faltinsen's linear solutions [13]. Using smaller time intervals or grid sizes, or adopting a tank ten times smaller, did not reduce solution differences significantly. Adjusting z_0, Δ, and CSL values led to the same result, indicating the presently adopted grid mesh was sufficient for numerical convergence and the viscosity terms could be ignored as for most sloshing flows. To identify if the sloshing flows were irrotational, as assumed by Faltinsen et al. [16], [17] for their analytical solution, Figure 6 shows the temporal variation of the normalized vorticity defined as $\Omega v/(Lc\omega^2)$, where vorticity $\Omega = \partial u/\partial z - \partial w/\partial x$. In Figures 6(a) and (b), which correspond to the ω/ω_0 values of 0.9 and 0.583, respectively, the time history of the normalized vorticity had a mean value of zero. Also, in spite of higher amplitudes, the curve in Figure 6(a) intersects with the abscissa more frequently than in Figure 6(b) within a given time period, implying that water flows with higher ω/ω_0 values were more likely to return to irrotation ($\Omega = 0$).
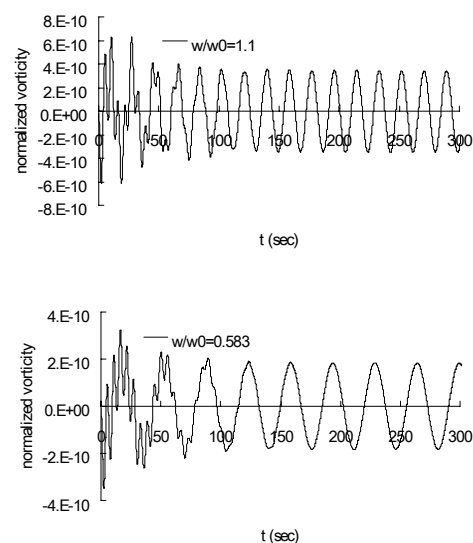
Fig. 6 A check on flow vorticities at
$x/L = 0, y/B = 0.5, \sigma = 1$ for various frequencies.

IV. APPLICATIONS

Following the essential tests mentioned above, the numerical method proposed in this paper was applied to further analyses of water flows confined in a rigid tank. The numerical experiment was broken down into six cases for discussion. The parameters applied to each case are recorded in Table V, and the calculation results or graphs derived are labeled as shown in Column 2, Table V.

Case 1 in Table V studied the water flow behavior in a tank moving horizontally at a constant acceleration. The results in Figure 7 show where each major variable (*u, w, p, H*) fluctuated with time after the water tank experienced such acceleration. Subfigure (a) indicates that the water flow in the center of the water tank gradually moved simultaneously with the water tank, and the relative velocity became zero at the end, which conformed to the fact. Subfigure (b) reveals that the vertical velocity at the sides of the tank was not high and became zero at the end, so the water flow became a steady-state flow. In subfigure (c), the maximum dynamic pressure was about 35000 N/m^2, equivalent to an hydrostatic pressure of 3.5 m (refer to subfigure (d)). This accounted for 35% of the total water depth, and therefore had a non-negligible influence on the nature of the overall water flow. Hence, the traditional hypothesis regarding hydrostatic pressure did not apply to this case, suggesting that this hypothesis be taken out of consideration during the simulation of a sloshing flow for this paper. Moreover, when $t \to \infty$, $a_x/g = dH/dx$, the final water level in the side middle of the tank was obtained as -500*1/250=-2.0 (m). This result conformed to the result obtained from the simulation shown in subfigure (d), thus confirming the accuracy of the numerical method. From this case, it was clear that the water level tended to stabilize through up-down oscillations, even in the case of
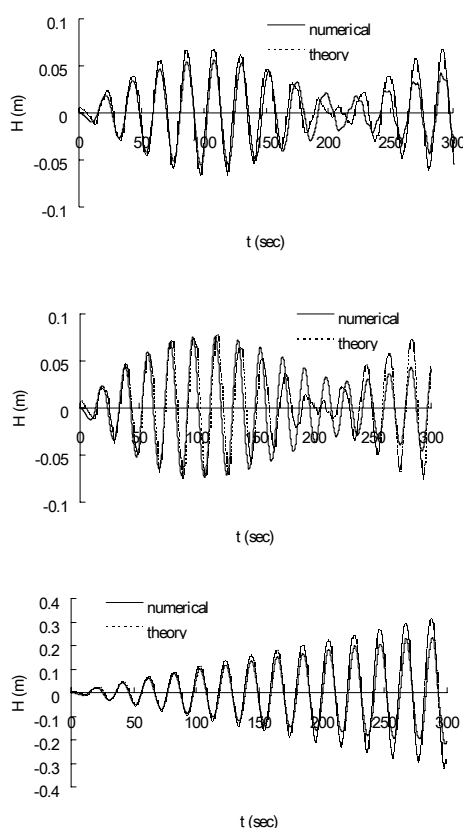

Fig. 5 Comparisons of the numerical results with the analytical solution based on Faltinsen's linear theory. $\omega/\omega_0 = 0.9$, 1.1, 0.99 for subfigures (a), (b), and (c), respectively.

World Academy of Science, Engineering and Technology
International Journal of Civil and Environmental Engineering
Vol:5, No:2, 2011

constant horizontal acceleration.

In Case 2, sloshing flows induced by a horizontal force equally imposed on the tank in the x and y directions were simulated. The force was represented by a sine wave-like horizontal acceleration which lasted three seconds, a situation similar to earthquakes. Since $du/dt = a_x$, the maximum u value in the center of the water tank should be $u_{max} = -2(3*0.5g/2\pi)$ = -4.68 (m/s), which was the same as the result obtained from the simulation. Figure 8(a) shows the result and presents a complete sine wave which formed within the first three seconds, thus implying the accuracy of the numerical method. In subfigure (b), although a sine wave pattern formed within the first three seconds, the pattern was slightly squeezed because the reflection waves interfered with the wave pattern at the sides of the tank. Afterwards, the wave alternated reasonably between positive and negative values. Subfigure (c) shows that the water levels at the middle of both sides of the tank were symmetrical on the time axis, simply proving the law of conservation of mass and the expected calculation results. It was discovered at the same time that the horizontal force caused a 10m high wave, approximately equal to an earthquake-induced tsunami. Subfigure (d) reveals that the dynamic pressure on the central surface of the tank was almost zero and did not vary with time. However, its absolute value gradually increased with depth. At the bottom of the tank, since w=0, the momentum equation on the z plane could be simplified as $\partial p/\partial z = 0$, meaning that the dynamic pressure distribution curve was parallel to the vertical axis at any given time. This also conformed to the simulation results.

To further test the robustness of our numerical algorithms, two large wind stresses of 1 and 8 N/m^2 were adopted for simulating wind-induced shear flows. The results are shown in Figures 9 and 10, corresponding to Cases 3 and 4, respectively.

The time-dependent profile in Figure 9 reflects the water level changes along the central line (y/B=0.5) of the water tank. Each subfigure shows the profile only one second away from that in its previous and next subfigures. It was observed that the water level near the sides of the water tank first rose over time (refer to subfigures (a) and (b)), and then decreased about 2.5 seconds later (refer to subfigure (c)). The decrease was attributed to the lack of sufficient vertical support for the continually accumulating water flow at the sides and its consequent collapse. In fact, as with previous cases, there was no other external force to make the water level rise in this case, except for the inertial force of the water flow itself. As a limited inertial force cannot support a constantly inclining water surface, the continually downward pulling force, resulting from gravity, caused the water level to descend at the end. The increase and decrease of the two forces resulted in complicated fluctuations on the surface, though no obvious change was seen in the center of the tank (refer to subfigure (b) in Figure 7), only a constantly inclining water surface (refer to the last three subfigures). This conformed to expectations, thus making shear flow different from sloshing flow. The overly

inclining water surface resulted in a reverse-phase wave form, due to the pulling force of gravity; as a result, the water level alternated between positive and negative inclining angles.

The calculation results shown in Figure 9 have been applied in Figure 10. In subfigure 10(a), the possibility of water circulation was examined, with each curve representing the x-component velocity profile in the center of the water tank. As the water surface velocity was positive and the internal velocity was negative, circulation appeared during the 20 seconds when shear stress was applied. The circulation followed a clockwise direction, which conformed to the real situation. In addition, as shown in subfigure (b), it was apparent that the water surface was not flat but uneven, with risings and fallings occurring alternately. This resulted in a transverse secondary flow that moved in the y-direction. As in subfigures (c) and (d), when the velocity v was negative for 0-10 seconds where y/B<0.5, the secondary flow moved to the center of the tank; when the velocity v was positive where y/B>0.5, the secondary flow moved to the center of the tank as well. Both curves were completely symmetrical, so it was natural that the water surface rose. About 10 seconds later, the secondary flow weakened, and then moved in a reverse direction, so water flowed from the center to both sides of the tank. Consequently, the water surface in the center descended between 10.5 seconds and 13.5 seconds, as in subfigure (b).

As in Figure 11, the shear stress applied, as in Figure 9, was increased from 1.0 N/m² to 8.0 N/m², and at the same time changes of the major variables (u, v, w, p & H) over time were drawn up. In this case, the shear stress was assumed to be the same in both x and y directions, and u & v in the center of the square tank would also be the same because of symmetry. In subfigure (a), the solid line (u) completely overlaps the dotted line (v), which responded to the aforesaid results and once again validated our numerical algorithms. Moreover, the speed reached 2 m/s, which was about three times the speed applied as in Figure 9 (0.7 m/s, but not shown). After a further look at the figure, the steady state had not been shown yet despite a period of 1,200 seconds. In subfigure (b), the maximum dynamic pressure was approximately 30 N/m², which was about equal to a hydrostatic pressure of 0.3 cm, showing that the dynamic pressure of any point at the corners was unimportant despite a high shear stress of 8 N/m². Subfigures (c) and (d) show the time-dependent profiles of H and w at the tank corners, respectively, which are much smaller than those in subfigures (e) and (f) in terms of figures, indicating that changes in the water level in the center of the tank sides were more rapid. The subfigure at the bottom left shows the longitudinal curve of the dynamic pressure in the center of the tank sides where the maximum value was about -1280 N/m², which was equal to an hydrostatic pressure of 13 cm. As this value was likely to be the highest dynamic pressure in the tank, the hypothesis regarding the hydrostatic pressure was possibly supported by shear flow, generally speaking. The subfigure at the bottom right shows changes in the water level at x/L=0.5 over time, and asymmetry between the curves was observed, which again indicated that the conservation of mass and

World Academy of Science, Engineering and Technology
International Journal of Civil and Environmental Engineering
Vol:5, No:2, 2011

numerical calculations were correct.

Based on the above-mentioned results, it was reasoned that compared with sloshing flow, the water level would rise only a little by means of high shear force (lower than 60 centimeters). Thus, wind setup alone was not worrisome. What would be a concern was the combination of wind shear with explosion, earthquakes, or moon gravity to form resonance, thus magnifying the existing wave (e.g. gravity wave) and, leading to disasters, as shown in Figure 12.

Subfigure (a) in Figure 12 shows the water level fluctuations caused by simple shear flows and sloshing flows. Subfigure (b) retains Faltensin's linear solution curve for the sloshing flow as in subfigure (a) for comparison purposes. It was thus found that when a wind shear of 8 N/m^2 and the horizontal acceleration in Case 1 were both applied to the water tank at the same time, the water level fluctuations were similar to the combined curves in subfigure (a). Since the shear effect was far greater than the sloshing effect within a short period of time (t<50 seconds) in terms of the mixed flow, the solid lines (representing mixed flow) in subfigure (b) similar to the dotted lines (representing shear flow) in subfigure (a) appeared. However, after 180 seconds, it was discovered that the water level had doubled because the solid and dotted curves in subfigure (a) were almost in-phase, leading to a higher water level than that between 70~150 seconds. Between 70~150 seconds, the reversed phase between the shear flow and sloshing flow made the water level of the mixed flow lower than that of a simple sloshing flow. In practice, the sloshing force chosen for this case was insignificant, as compared with a wind shear of 8 N/m^2 in real life. Both forces however, made about the same contribution to the change of water elevation. Thus, wind shears must be large enough in order to interfere with a small sloshing wave, unless a much smaller C_{SL} is adopted.

Now, it could be inferred that the numerical model and method adopted in this paper were reasonable. The possible range of the major parameters was determined to effectively simulate the mixed flow which occurred when wind shear and sloshing force both applied. The key hypotheses regarding hydrostatic pressure and irrotational flow were not considered, so as to make the numerical method as general as possible. In this paper, the bottom of the water tank served as the horizon. Because the numerical method adopted was under initial testing and the higher order system differential equation was quite complicated, an irregularly changing bed was unsuitable for the current phase, to avoid loss of focus on the core of the question. In the future, the coordinate transformation formula will be revised, and the temporal and special variation of the bed will be included for a more complete method. Comparatively speaking, the numerical method used in this paper obtained good results in the case of coarse grids (with only 11*11 nodes in the horizontal direction), with a larger time interval. The matrix equation used in this paper was penta-diagonal, and could be immediately solved using back substitution. Unlike high-dimensional matrix equations in x-y-z geometry, this equation was easily constructed and efficiently solved. However, due to horizontal decoupling of the numerical model, the numerical structure proposed in this paper was only applicable to shallow water areas where the water depth was far lower than the horizontal dimension of the water area (for example, L/D<0.1 and B/D<0.1). Fortunately, shallow water areas are very common, so this limitation would not be problematic in actual situations.

TABLE V CONVERGENCE STUDY

Case	for	flow dimensions (m)			node number			Δt (sec)
		L	B	D	x	y	z	
1	fig.7	1000	1000	100	21	11	31	1.0
2	fig.8	1000	1000	100	11	11	31	0.3
3	fig.9, 10	1000	500	100	31	21	31	0.5
4	fig.11	1000	1000	100	11	11	31	1.0
5	fig.12	100	100	10	11	11	31	0.15

TABLE V CONVERGENCE STUDY (CONT.)

Case	C_{sL}/C_{sL0}	a_x	a_y	τ_x	τ_y	ω/ω_0	c/D
1	0.05	$-g/250$	0	0	0	--	--
2	0.05	$-0.5g\sin\left(\dfrac{2\pi t}{3}\right), t \le 3 \,,\, 0 \,,\, t > 3$	$= a_x$	0	0	--	--
3	0.05	0	0	1.0	0	--	--
4	0.05	0	0	8.0	8.0	--	--
5	0.01	$c\omega^2\sin\omega t$	0	8.0	0	0.9	0.00183

World Academy of Science, Engineering and Technology
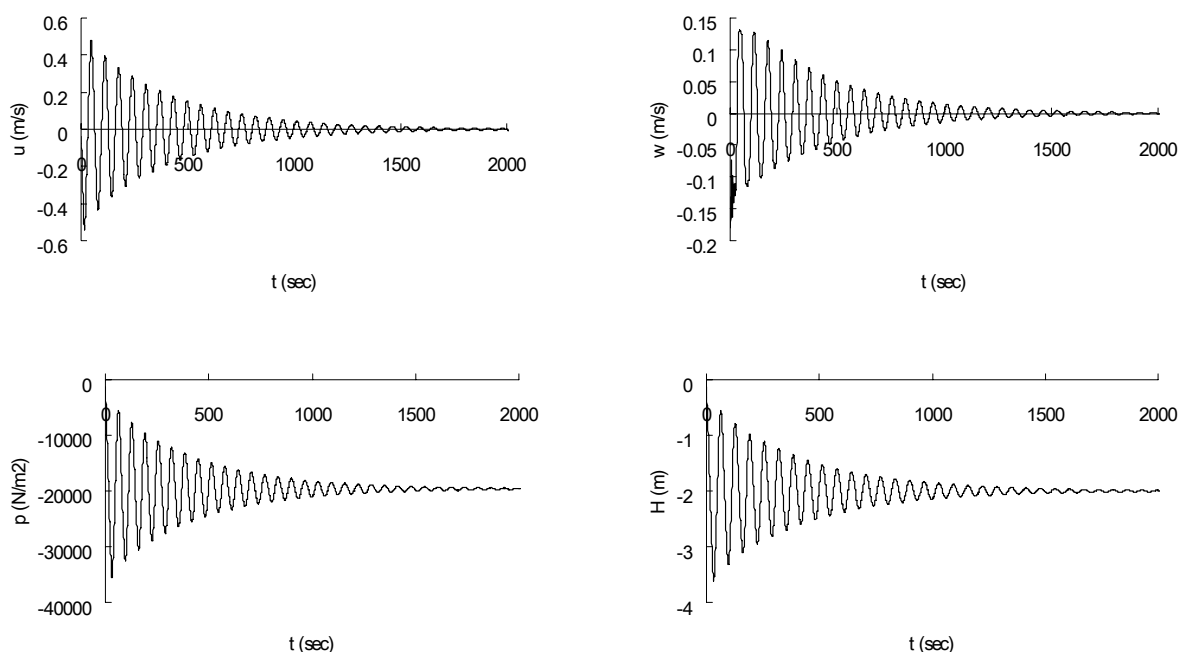International Journal of Civil and Environmental Engineering
Vol:5, No:2, 2011

Fig. 7 History of the target variables under the action of a constant horizontal acceleration; the position of each subfigure: (a) $x/L = 0.5, y/B = 0.5, \sigma = 1$; (b) $x/L = 1, y/B = 0.5, \sigma = 1$; (c) $x/L = 1, y/B = 0.5, \sigma = 0$; (d) $x/L = 1, y/B = 0.5$.
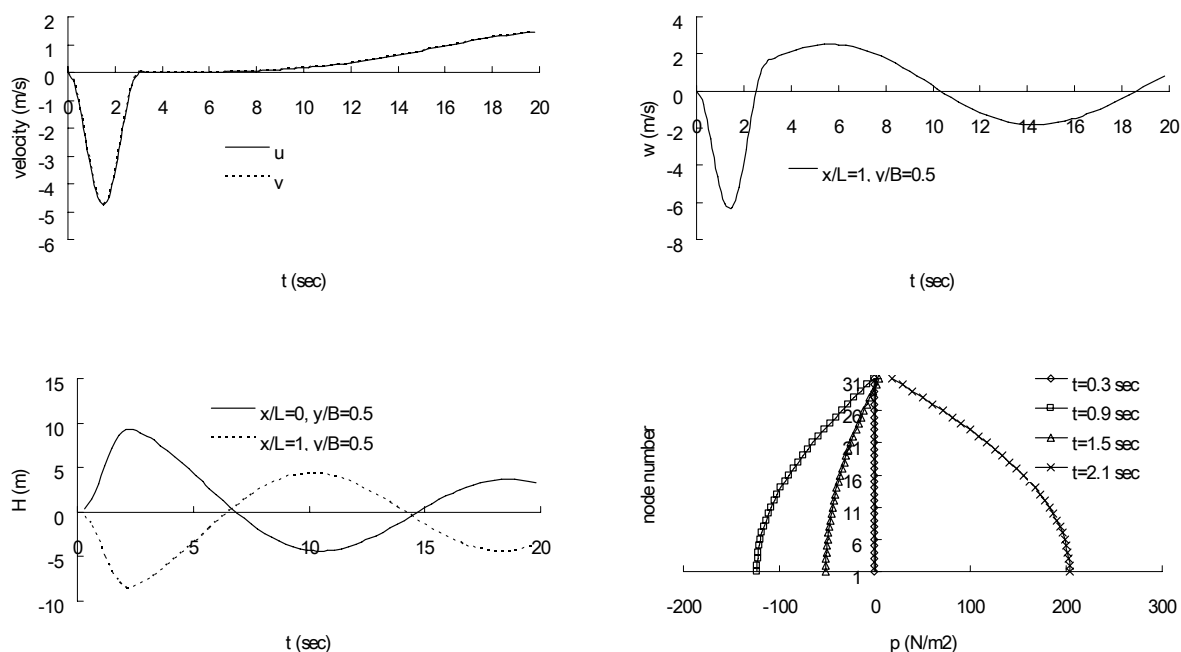

Fig. 8 History of the target variables due to a sine wave-like horizontal acceleration lasting three seconds; the position of each subfigure: (a) $x/L = 0.5, y/B = 0.5, \sigma = 1$; (b) $x/L = 1, y/B = 0.5, \sigma = 1$; and (d) $x/L = 0.5, y/B = 0.5$

World Academy of Science, Engineering and Technology
International Journal of Civil and Environmental Engineering
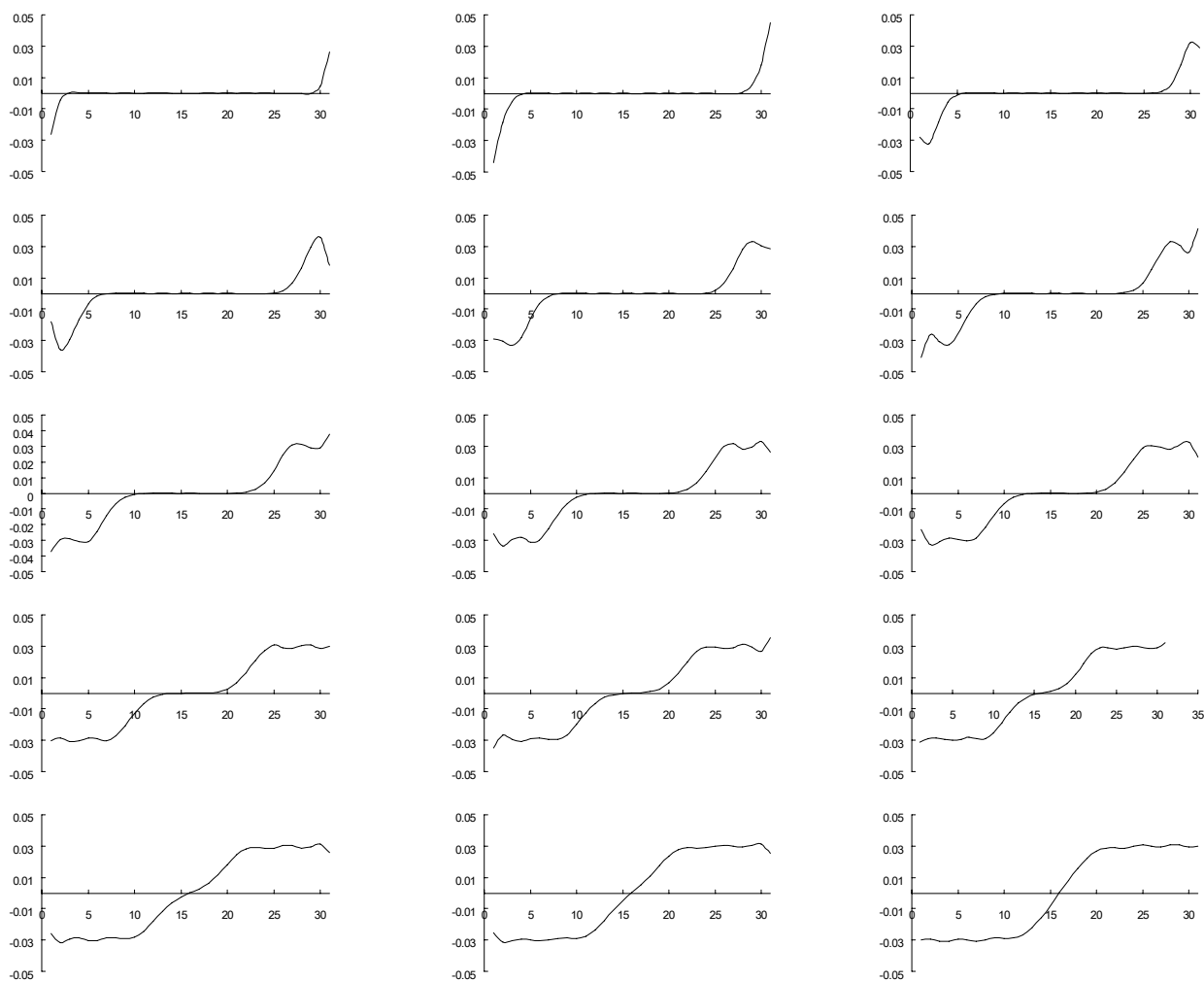Vol:5, No:2, 2011

Fig. 9 Snapshots of the free water surface, starting at t=0.5 seconds and then taken at every second (from left to right and up to down); the position of each subfigure: $y / B = 0.5$ (ordinate: water elevation in meter, abscissa: node numbers in x direction)
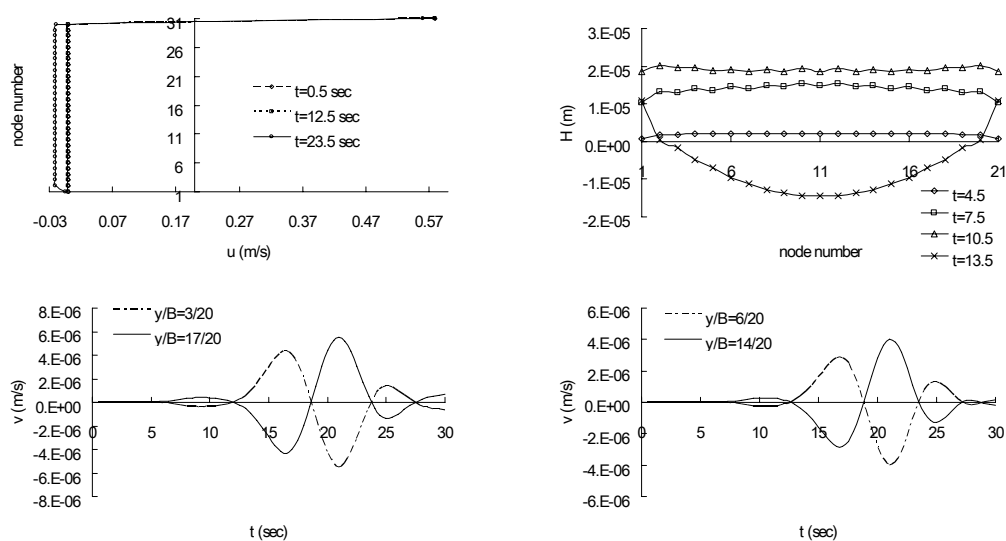

Fig. 10 Test of the existence of secondary flows due to a wind shear of 1.0 N/m²; the position of each subfigure: (a) $x / L = 0.5$; (b) $x / L = 0.5$, $y / B = 0.5$; and (c) and (d) $x / L = 0.5$, $\sigma = 1$

World Academy of Science, Engineering and Technology
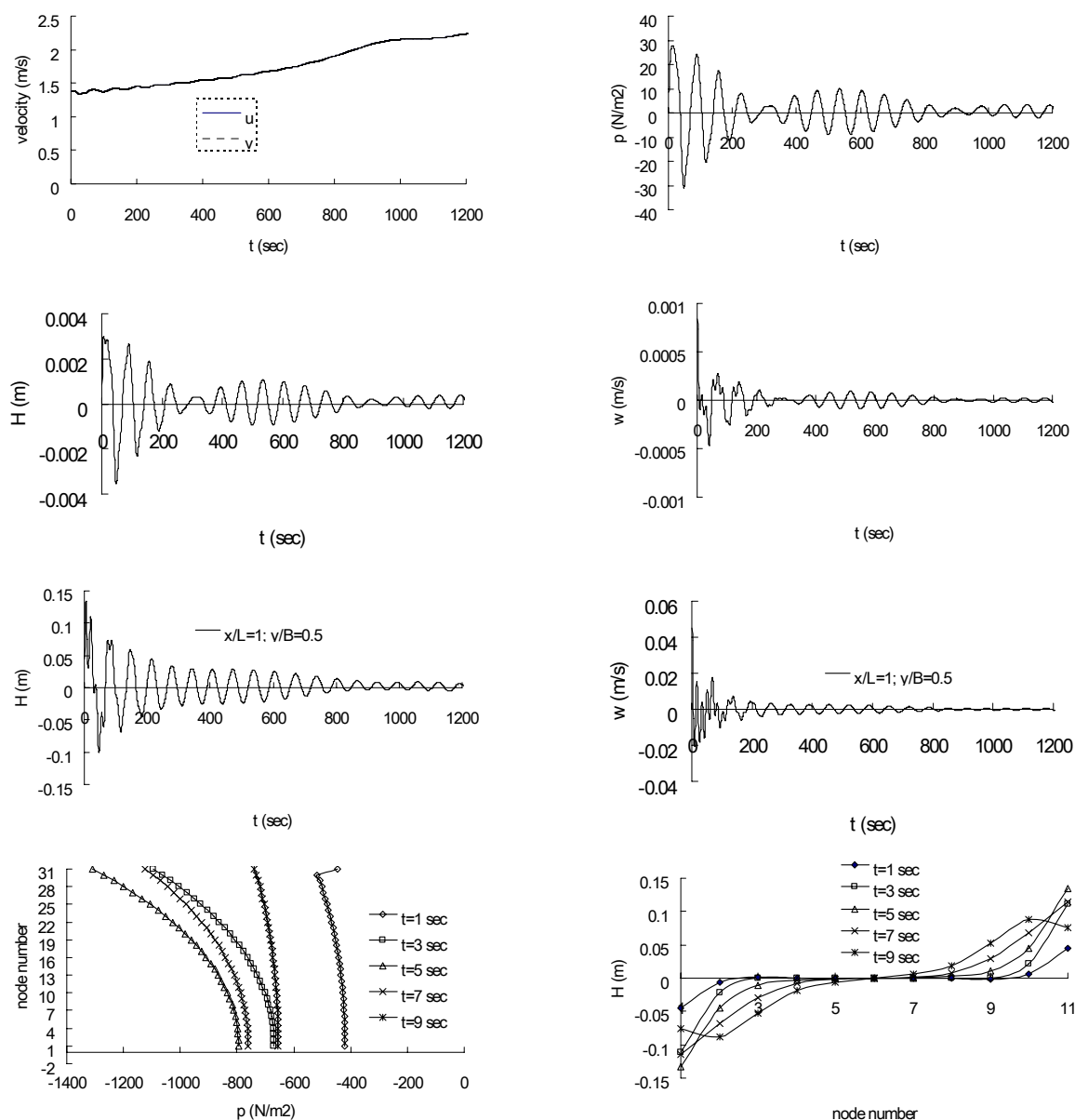International Journal of Civil and Environmental Engineering
Vol:5, No:2, 2011

Fig. 11 History of the target variables under a constant wind stress action; the position of each subfigure:
(a) and (f) $x/L = 0.5, y/B = 0.5, \sigma = 1$; (b) $x/L = 1, y/B = 1, \sigma = 0$; (c) $x/L = 1, y/B = 1$;
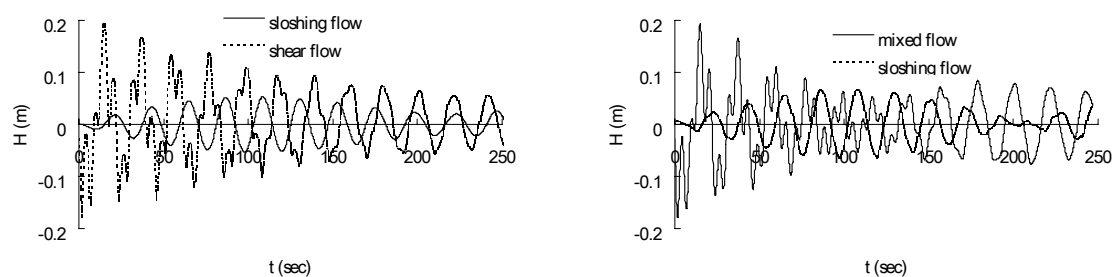(d) $x/L = 1, y/B = 1, \sigma = 1$; (e) $x/L = 1, y/B = 0.5$; (g) $x/L = 0, y/B = 0.5$; and (h) $y/B = 0.5$.

Fig. 12 History of the water elevation for different types of flow; the position of each subfigure:
(a) $x/L = 0, y/B = 0.5$; and (b) $x/L = 0, y/B = 0.5$ (all curves except the dash line in (b) are from simulations).

World Academy of Science, Engineering and Technology
International Journal of Civil and Environmental Engineering
Vol:5, No:2, 2011

V. CONCLUSIONS

This part of study validated of our models through the comparisons of numerical and analytical solutions. Involved mathematic manipulations became much less after transforming the full 3-D STF Navier-Stokes equations into a group of horizontally "decoupled" 1-D equations. This not only rendered parallel computations amenable, but also allows the inclusion of those well-developed 1-D algorithms that avoided node-to-node spurious numerical oscillations. All the benefits made it potentially superior to other methods ready for solving the 3-D fluid flow problems.

It was found possible for C_{SL} to become much smaller than 0.17, as adopted by several researchers, when waters were very shallow and grids were coarse. For the present tank scales, water elevation rose less than one meter when subjected to wind shears alone. It was achieved easily, however, by shaking the tank with a small horizontal acceleration, implying the danger for people standing next to a dam during an earthquake. With only a small deviation from the hydrostatic assumption, the wind-induced shear flow had a strong correlation with the C_{SL} value. The sloshing flow, however, was independent of it and showed significantly large dynamic pressure when the water moved back and forth. In sloshing-shear mixed flows, the resulting amplitude of the water elevation was found to be suppressed or amplified, as compared with the sloshing force alone. Shear forces were therefore not always negligible in shallow fluid bodies. In spite of the sparsely distributed grid nodes, competitively accurate results were obtained for the model validation and robustness test. The numerical strategy proposed in the paper worked well, especially for very shallow waters ($L/D<0.1$ and $B/D<0.1$) on a large scale.

REFERENCES

[1] D. K. Lilly, "The representation of small-scale turbulence in numerical simulation experiments," Proc. IBM Sci. Comput. Symposium Environ. Sci., IBM Data Process Div., White Plains, N.Y., pp. 195-210, 1967.

[2] J. W. Deardorff, "A numerical study of three-dimensional turbulent channel flow at large Reynolds numbers," J. Fluid Mech., vol. 41, pp. 453-480, 1970.

[3] P. J. Mason, and N. S. Callen, "On the magnitude of the subgrid-scale eddy coefficient in large eddy simulations of turbulent channel flow," J. Fluid Mech., vol. 162, pp. 439-462, 1986.

[4] J. Constantin, M. G. Inclan, and M. Raschendorfer, "The energy budget of a spruce forest: field measurements and comparison with the forest-land-atmosphere model (FLAME)," J. of Hydrology, pp. 212-213, 22-35, 1998.

[5] C. Babajimopoulos, and K. Bedford, "Formulating lake models with preserve spectral statistics," J. Hydr. Div., ASCE, vol. 106, pp. 1-19, 1980.

[6] H. Schmidt, and U. Schumann, "Coherent structure of the convective boundary layer derived from large-eddy simulations," J. of Fluid Mech., vol. 200, pp. 511-565, Great Britain. 1989.

[7] C. B. Liao, M. F. Wu, and M. H. Gou, "Large eddy simulation of a round jet in a cross flow," Proceedings of the 13th hydraulic engineering conference, M14-M21, Taiwan. 2002.

[8] W. H. Chung, "Dependence of the Smagorinsky-Lilly's constant on inertia, wind stress, and bed roughness for large eddy simulations," Journal of Mechanics, vol. 22, No. 2, pp. 125-136, 2006.

[9] G. T. Csanady, "Circulation in the Coastal Ocean," pp. 279, D. Reidel Pub. Co.., 1982.

[10] J. Amorocho, and J. J. Devries, "A new evaluation of the wind stress coefficient over water surfaces," J. Geophys. Res., vol. 85, pp. 433-442, 1980.

[11] W. H. Chung, "Dependence of the Smagorinsky-Lilly's constant on inertia, wind stress, and bed roughness for large eddy simulations," Journal of Mechanics, vol. 22, No. 2, pp. 125-136, 2006.

[12] O. M. Faltinsen, "A numerical non-linear method of sloshing in tanks with two-dimensional flow," J. of Ship Research, vol. 18(4), pp. 224-241, 1978.

[13] T. M. Okamoto, and M. Kawahara, "Two-dimensional sloshing analysis by Lagrangian finite element method," International Journal for Numerical Methods in Fluids, vol. 11, pp. 453-477, 1990.

[14] W. Chen, M. A. Haroun, and F. Liu, "Large amplitude liquid sloshing in seismically excited tanks," Earthquake Engineering and Structural Dynamics, vol. 25, pp. 653-669, 1996.

[15] G. X. Wu, Q. W. Ma, and R. E. Taylor, "Numerical simulation of sloshing waves in a 3D tank based on a finite element method," Applied Ocean Research, vol. 20, pp. 337-355, 1998.

[16] O. M. Faltinsen, O. F. Rognebakke, and A. N. Imokha, "Resonant three-dimensional nonlinear sloshing in a square-base basin, Part 2. Effect of higher modes," J. Fluid Mech, vol. 523, pp. 199-218, 2002.

[17] O. M. Faltinsen, O. F. Rognebakke, and A. N. Timokha, "Transient and steady-state amplitudes of resonant three-dimensional sloshing in a square base thank with a finite fluid depth," Physics of Fluids, vol. 18, 012103, pp. 1-14, 2006.

Dr. Weihao-Chung received his Ph. D. from the Department of Civil Engineering & Operations Research, Princeton University, U.S.A., in 1994. He has served over ten years in Civil Engineering Department, Chinese Military Academy, Taiwan, since 1998. Being an associate professor presently, his research areas include: open channel flow, hydrology analysis, fluid flow simulations by STF technique, groundwater hydrology, water evaporation and infiltration in bare soils, etc.

Mr. Iau-Teh Wang received his Master's degree in Military Engineering, Chung-Cheng Institute of Technological, Taiwan, R.O.C. in 2004, and is presently a postgraduate student pursuing his Ph.D. degree at Graduate Institute of Disaster Prevention on Hillslopes and Water Resources Engineering, National Pingtung University of Science and Technology. Being a lecturer in the Department of Civil Engineering, Chinese Military Academy, Taiwan, he focuses on slope stability problems and underground engineering.

Yu-hsi Hu received her MA. from Department of Curriculum & Instruction, University of Kansaa, U.S.A., in 1991. Since then, she has been devoting herself to writing and language translation in Department of Applied English, Tajen University, Taiwan. She, being a lecturer presently, specializes in TESOL and translation.